Modeling NH_4NO_3 over the San Joaquin Valley during the 2013 DISCOVER-AQ campaign

James T. Kelly[1], Caroline L. Parworth[2,3], Qi Zhang[2,3], David J. Miller[4], Kang Sun[5], Mark A. Zondlo[6], Kirk R. Baker[1], Armin Wisthaler[7], John B. Nowak[8], Sally E. Pusede[9], Ronald C. Cohen[10], Andrew J. Weinheimer[11], Andreas J. Beyersdorf[12], Gail S. Tonnesen[13], Jesse O. Bash[14], Luke C. Valin[14], James H. Crawford[8], Alan Fried[15], and James G. Walega[15]

[1]U.S. Environmental Protection Agency, Office of Air Quality Planning & Standards, RTP, NC
[2]Department of Environmental Toxicology, University of California, Davis, CA
[3]Agricultural and Environmental Chemistry Graduate Group, University of California, Davis, CA
[4]Environmental Defense Fund, Boston, MA
[5]Atomic and Molecular Physics Division, Harvard-Smithsonian Center for Astrophysics, Cambridge, MA
[6]Department of Civil and Environmental Engineering, Princeton University, Princeton, NJ
[7]Institute for Ion Physics and Applied Physics, University of Innsbruck, Innsbruck, Austria
[8]National Aeronautics and Space Administration, Langley Research Center, Hampton, VA
[9]Department of Environmental Sciences, University of Virginia, Charlottesville, VA
[10]Department of Earth and Planetary Sciences, University of California at Berkeley, Berkeley, CA
[11]National Center for Atmospheric Research, Boulder, CO
[12]Department of Chemistry and Biochemistry, California State University, San Bernardino, CA
[13]U.S. Environmental Protection Agency, Region 8, Denver, CO
[14]U.S. Environmental Protection Agency, Office of Research and Development, RTP, NC
[15]Institute of Arctic and Alpine Research, University of Colorado, Boulder, CO 80309, USA
Corresponding author: James T. Kelly, Tel: 919-541-0886, Email: kelly.james@epa.gov

Abstract

The San Joaquin Valley (SJV) of California experiences high concentrations of $PM_{2.5}$ (particulate matter with aerodynamic diameter ≤ 2.5 μm) during episodes of meteorological stagnation in winter. Modeling $PM_{2.5}$ NH_4NO_3 during these episodes is challenging because it involves simulating meteorology in complex terrain under low wind speed and vertically stratified conditions, representing complex pollutant emissions distributions, and simulating daytime and nighttime chemistry that can be influenced by the mixing of urban and rural air masses. A rich dataset of observations related to NH_4NO_3 formation was acquired during multiple periods of elevated NH_4NO_3 during the DISCOVER-AQ (Deriving Information on Surface Conditions from Column and Vertically Resolved Observations Relevant to Air Quality) field campaign in SJV in January and February 2013. Here, NH_4NO_3 is simulated during the SJV DISCOVER-AQ study period with the Community Multiscale Air Quality (CMAQ) model version 5.1, predictions are evaluated with the DISCOVER-AQ dataset, and process analysis modeling is used to quantify HNO_3 production rates. Simulated NO_3^- generally agrees well with routine monitoring of 24-h average NO_3^-, but comparisons with hourly average NO_3^- measurements in Fresno revealed differences at higher time resolution. Predictions of gas-particle partitioning of total nitrate (HNO_3 + NO_3^-) and NHx (NH_3 + NH_4^+) generally agreed well with measurements in Fresno, although partitioning of total nitrate to HNO_3 was sometimes overestimated at low relative humidity in afternoon. Gas-particle partitioning results indicate that NH_4NO_3 formation is

limited by HNO_3 availability in both the model and ambient. NH_3 mixing ratios are underestimated, particularly in areas with large agricultural activity, and the spatial allocation of NH_3 emissions could benefit from additional work, especially near Hanford. HNO_3 production via daytime and nighttime pathways is reasonably consistent with the conceptual model of NH_4NO_3 formation in SJV, and production peaked aloft between about 160 and 240 m in the model. During a period of elevated NH_4NO_3, the model predicted that the OH + NO_2 pathway contributed 46% to total HNO_3 production in SJV and the N_2O_5 heterogeneous hydrolysis pathway contributed 54%. The relative importance of the OH + NO_2 pathway for HNO_3 production is predicted to increase as NOx emissions decrease.

1. Introduction

The San Joaquin Valley (SJV or Valley) makes up the southern portion of California's Central Valley and is formed by the coastal mountain ranges in the west, the Sierra Nevada mountains in the east, and the convergence of mountain ranges in the south at the Tehachapi mountains. SJV is about 400 km long and 60-100 km wide and includes parts or all of eight counties having a combined population of about 4.2 million [*CDOF*, 2017]. The Valley population is projected to increase rapidly in coming decades, by ~60% from 2016 to 2060 [*CDOF*, 2017], which has implications for air quality planning [*Hixson et al.*, 2012]. SJV contains major cities such as Fresno (pop. ~520,000) and Bakersfield (pop. ~380,000), important oil and gas fields [*CDOC*, 2015; *Gentner et al.*, 2014], and an extremely productive agricultural region [*CDFA*, 2016a]. For instance, SJV had about 1.5 million dairy cows and produced about 36 billion pounds of milk in 2016 [*CDFA*, 2016b]. The Valley is also a major north-south corridor for goods transport along Highway 99 in the east and Interstate 5 in the west. SJV's terrain combined with pollutant emissions from the large population and economic activity leads to high concentrations of $PM_{2.5}$ (particulate matter with aerodynamic diameter ≤2.5 μm), particularly during periods of stagnant meteorology in winter months. SJV is in nonattainment of U.S. EPA's primary national ambient air quality standards for $PM_{2.5}$ that are set to protect public health.

Air pollution in SJV has been studied for decades, and conceptual models of wintertime $PM_{2.5}$ formation in SJV have been developed, largely based on the 1995 Integrated Monitoring Study and the 2000/2001 California Regional PM_{10}/$PM_{2.5}$ Air Quality Study (CRPAQS) [*Herner et al.*, 2005; *Herner et al.*, 2006; *Pun and Seigneur*, 1999; *Watson and Chow*, 2002; *Watson et al.*, 1998]. Briefly, high pressure systems over the Great Basin lead to subsidence temperature inversions over the Valley that limit daytime mixing heights from less than 400 to ~800 m for periods of days to more than a week. Radiation temperature inversions

also form overnight and limit mixing of surface emissions to a ~30-50 m layer that is decoupled from the residual layer above. Primary carbonaceous particles are concentrated in the shallow nighttime surface layer. Between the radiation inversion and the subsidence inversion, air masses rich in oxides of nitrogen, largely from urban areas and major highways, mix with air masses rich in NH_3, largely from rural agricultural areas, in a valley-wide layer overnight. Ammonium nitrate (NH_4NO_3) forms in this layer and mixes to the surface in the morning when the radiation inversion breaks. Morning increases in NH_4NO_3 at the surface therefore tend to coincide with decreases in carbonaceous $PM_{2.5}$. NH_4NO_3 makes up a large fraction of fine particle mass during major $PM_{2.5}$ episodes [e.g., *L W A Chen et al.*, 2007; *Chow et al.*, 2006; *Ge et al.*, 2012a; *Herner et al.*, 2005; *SJVAPCD*, 2012]. Persistent radiation fogs also occur in SJV in wintertime, and the chemistry of fine particles can be influenced by aqueous-phase processes [e.g., *Collett et al.*, 1999a; *Collett et al.*, 1999b; *Ge et al.*, 2012b; *Herckes et al.*, 2015; *Jacob et al.*, 1986].

Air quality models have been used in combination with the CRPAQS dataset to better understand air pollution processes in SJV. Overall, models did a reasonable job of predicting PM during CRPAQS [*Kelly et al.*, 2011; *Pun et al.*, 2009; *Ying et al.*, 2008a; *Y Zhang et al.*, 2010] and were used to provide information on process rates, visibility impairment, and source apportionment and regional contributions to primary and secondary PM [*J Chen et al.*, 2009; 2010; *Ying*, 2011; *Ying and Kleeman*, 2009; *Ying et al.*, 2008b; *Ying et al.*, 2009]. Air quality models have also been used to understand the impact of precursor emissions on NH_4NO_3 [*Blanchard et al.*, 2000; *J Chen et al.*, 2014; *Kleeman et al.*, 2005; *Livingstone et al.*, 2009; *Pun et al.*, 2009; *Pun and Seigneur*, 2001; *Stockwell et al.*, 2000]. Generally, these studies found that NOx ($NO + NO_2$) emission reductions would be the most effective emission control for reducing NH_4NO_3 in SJV. Air quality management strategies based on in part on NOx emission reductions, which are also important for reducing ozone in the Valley, have been implemented [e.g., *SJVAPCD*, 2012; *SJVAPCD*, 2016].

The studies discussed above were largely based on $PM_{2.5}$ episodes that occurred one to two decades ago. Although these studies are still relevant, air quality has improved over time in SJV due to reductions in NOx and other emissions [e.g., *McDonald et al.*, 2012; *Pusede and Cohen*, 2012; *Pusede et al.*, 2016; *Pusede et al.*, 2014; *Russell et al.*, 2012]. The DISCOVER-AQ (Deriving Information on Surface Conditions from Column and Vertically Resolved Observations Relevant to Air Quality) campaign in January and February of 2013 provides a rich dataset for more recent wintertime $PM_{2.5}$ episodes in SJV. Peak $PM_{2.5}$ concentrations were lower during DISCOVER-AQ than CRPAQS, but NH_4NO_3 still made up a large fraction of fine particle mass consistent with the earlier study. The DISCOVER-AQ dataset has recently been used to investigate $PM_{2.5}$ precursor emissions and formation processes in SJV [e.g., *Miller et al.*, 2015; *Parworth et al.*, 2017; *Prabhakar et al.*, 2017; *Pusede et al.*, 2016; *Shephard and Cady-Pereira*, 2015; *Sun et al.*, 2015; *Young et al.*,

2016; *X L Zhang et al.*, 2016]. In particular, Pusede et al. [2016] used the DISCOVER-AQ dataset in combination with the historical monitoring record to interpret past trends and predict future trends in NH_4NO_3 in SJV. They found that NH_4NO_3 formation is limited by NOx emissions, both daytime and nighttime formation pathways are important, and predict that the daytime pathway will become increasingly important in the future.

Previous studies using the 2013 SJV DISCOVER-AQ dataset were generally based on conceptual, analytical, and box modeling in combination with the measurements. Compared with earlier field campaigns, limited regional photochemical modeling has been done for SJV DISCOVER-AQ. Regional photochemical modeling is valuable because it provides comprehensive information on key processes in three-dimensions across the entire region for the entire period and is constrained by relatively few assumptions. The lack of constraints in air quality modeling is advantageous for exploring alternative scenarios but requires that models be thoroughly evaluated to insure they adequately reflect ambient processes. Modeling $PM_{2.5}$ episodes in SJV is particularly challenging because it involves simulating meteorology in complex terrain under low wind speed and vertically stratified conditions, representing complex pollutant emissions distributions, and simulating daytime and nighttime chemistry that can be influenced by the mixing of urban and rural air masses. Reliable modeling of $PM_{2.5}$ in SJV is important, however, to help inform air quality management for the highly populated nonattainment area. Here, the DISCOVER-AQ dataset is used to perform a thorough evaluation of regional photochemical modeling of NH_4NO_3 in the Valley during January and February 2013. Process analysis modeling is also conducted to help interpret model predictions and contribute to the understanding of air pollution in the Valley.

2. Methods

2.1 Modeling

Photochemical grid modeling was performed with the Community Multiscale Air Quality (CMAQ; www.epa.gov/cmaq) model version 5.1 [*Appel et al.*, 2017] on a domain covering SJV from south of the Tehachapi mountains to north of Sacramento and parts of the Sierra Nevada mountains in the east and Pacific Ocean in the west (Figure S1). The CMAQv5.1 simulations were configured with integrated reaction rate and process analysis [*Jang et al.*, 1995; *Jeffries and Tonnesen*, 1994; *Kim et al.*, 2014] and covered the 4 January – 10 February 2013 period. Horizontal grid resolution of 4 km was used with 35 vertical layers that matched the vertical structure of the meteorological model. Chemical boundary conditions were developed from a CMAQv5.1 simulation that covered the contiguous U.S. and surrounding areas with 12-km horizontal resolution. NH_3 surface exchange was simulated with CMAQ's bi-directional exchange

parameterization [*Bash et al.*, 2013; *Pleim et al.*, 2013], and gas-phase chemistry was parameterized with the CB05e51 mechanism [*Appel et al.*, 2017]. Inorganic aerosol thermodynamics were simulated with ISORROPIA II [*Fountoukis and Nenes*, 2007] in metastable mode, where crystallization does not occur. Semi-volatile inorganic particle components (i.e., NO_3^-, NH_4^+, Cl^-) in the Aitken and accumulation modes are assumed to be in bulk equilibrium with their gas-phase counterparts (i.e., HNO_3, NH_3, and HCl) in CMAQ, whereas diffusive mass transfer is explicitly simulated for semi-volatile coarse-mode particle components [*Kelly et al.*, 2010]. Heterogeneous hydrolysis of N_2O_5 on Aitken- and accumulation-mode particles is based on *Davis et al.* [2008], and N_2O_5 hydrolysis on coarse-mode particles is based on *Bertram and Thornton* [2009] as described by *Sarwar et al.* [2012].

Gridded emission fields for CMAQ modeling were developed with the Sparse Matrix Operator Kernel Emissions (SMOKE) model [*Houyoux et al.*, 2000] version 3.7. The emissions modeling procedures used here are similar to those described in detail previously for national 12-km resolution modeling [*USEPA*, 2017b]. Point source emissions were based on 2013 continuous emissions monitoring (CEM) data when available and state submitted data otherwise. Anthropogenic non-point source emissions were based on version 2 of the 2011 National Emission Inventory (NEI11v2) [*USEPA*, 2016]. Onroad mobile source emission totals by county were estimated by interpolating totals from 2011 and 2014 based on EMFAC2014 (www.arb.ca.gov/emfac/) modeling by the California Air Resources Board (CARB). The interpolated onroad emission totals were then temporally and spatially allocated using results of a MOVES2014a (Motor Vehicle Emission Simulator; www.epa.gov/moves) simulation according to a hybrid procedure described previously [*USEPA*, 2012b; 2017b]. Offroad mobile source emission totals were also based on information provided by CARB. The Biogenic Emission Inventory System (BEIS) version 3.61 was used with the Biogenic Emissions Landuse Database (BELD) version 4.1 to estimate biogenic NO and speciated VOC emissions [*Bash et al.*, 2016]. NH_3 emissions from livestock and fertilizer application were based on NEI11v2 annual county totals that were allocated to hour of day using 2013 temperature data [*USEPA*, 2016].

The Weather Research and Forecasting (WRF) model [*Skamarock et al.*, 2008] version 3.7 was used to generate gridded meteorological fields for CMAQ and SMOKE. WRFv3.7 was applied with 35 vertical layers from the surface to 50 mb with higher resolution near the surface to better resolve the planetary boundary layer (PBL). Key physics options used in the WRF simulation include the Pleim-Xiu land surface model [*Pleim and Xiu*, 2003], asymmetric convective mixing model version 2 [ACM2; *Pleim*, 2007], RRTMG short and longwave radiation parameterization [*Mlawer et al.*, 1997], and Morrison two-moment microphysics scheme [*Morrison et al.*, 2009].

2.2 Measurements

Measurements of NH_3, TNO3 (HNO_3 + fine particle NO_3^-), NO, NO_2, NOy (oxides of nitrogen including NOx, HNO_3, HNO_4, HONO, NO_3 radical, organic nitrates, and N_2O_5), O_3, and HCHO made from the NASA P-3B aircraft during daytime flights on 16, 18, 20-22, and 30-31 January and 1, 4, and 6 February 2013 are used to examine model performance. The aircraft flew 2-3 repeated circuits per day over SJV including vertical spiral trajectories with ~5-km diameters over six sites (i.e., Bakersfield, Hanford, Tranquility, Fresno, Huron, and Porterville). NH_3 was measured with a cavity ring down spectrometer (CRDS; G2103, Picarro Inc.) and a proton-transfer-reaction time-of-flight mass spectrometer (PTR-ToF-MS). Measurements from these instruments have been compared previously and were found to provide complementary information [*Sun et al.*, 2015]. Therefore both the CRDS and PTR-ToF-MS measurements are used here. TNO3 was measured on the P-3B aircraft by thermal dissociation of ambient NOy species followed by laser-induced fluorescence of NO_2. Specifically, TNO3 was calculated as NO_2 measured in the 600°C channel minus that measured in the 400°C channel with correction for slight conversion of HNO_3 in the alkyl nitrate channel [*Pusede et al.*, 2016; *Womack et al.*, 2017]. NO, NO_2, O_3, and NOy were measured with the National Center for Atmospheric Research (NCAR) four-channel chemiluminescence instrument. The NOy measurement likely includes some contribution from NO_3^- in sub 1-μm particles, although the amount of contribution is uncertain. Airborne size distributions of particles with diameters between 90 and 7500 nm were measured with a Laser Aerosol Spectrometer (LAS, TSI Inc.) calibrated with polystyrene latex spheres. Airborne measurements of aerosol composition by a particle-into-liquid sampler (PILS) and offline ion chromatography (IC) analysis showed that nitrate constituted 53% of the water-soluble aerosol mass. HCHO was measured with difference frequency generation absorption spectroscopy [*Weibring et al.*, 2006]. P-3B measurements were acquired from Revision 4 merged files available in the NASA online database [*NASA*, 2017].

NH_3 was also measured from a mobile ground laboratory that sampled conditions across the Valley during transects on 21-22 and 25-31 January and 1, 3-5, and 7 February 2013. Mobile measurements were performed with an open-path, quantum-cascade laser-based sensor mounted on the roof rack of a sedan passenger car [*Miller et al.*, 2014; *Sun et al.*, 2014] as described previously [*Miller et al.*, 2015; *Sun et al.*, 2015]. Mobile laboratory data were acquired from Revision 0 files available online [*NASA*, 2017]. At the CARB Fresno-Garland site, water soluble inorganic PM3 component ions including NO_3^-, NH_4^+, SO_4^{2-}, and K^+ were measured with sub-hourly resolution during 19 January to 10 February using a PILS-IC instrument, and water soluble gases including HNO_3 and NH_3 were collected with ~5-7 h resolution using annular denuders and analyzed offline by IC [*Parworth et al.*, 2017]. These data were acquired directly from the authors *Parworth et al.* [2017], although the data are also available online [*NASA*, 2017]. Meteorology

measurements collected by CARB were acquired from *NASA* [2017], radar profiler measurements at Visalia were obtained from *NOAA* [2017], and 24-h average $PM_{2.5}$ NO_3^- concentrations at SJV monitoring sites were obtained directly from CARB, although routine monitoring data are also available online [*USEPA*, 2017a].

2.3 Model-measurement pairing

Model predictions were generally paired with measurements according to standard practice by extracting predictions from the grid cell containing the measurement and then averaging the hourly model output to the sampling period of the measurement. To match model predictions with P-3B and mobile laboratory measurements, the grid cell containing the measurement at each second was identified, and predictions from that cell were linearly interpolated to the time of the measurement. The paired 1-s data were then averaged to 10-s resolution for the boxplot comparisons below. For spatial comparisons of CMAQ predictions with mobile laboratory NH_3 measurements, medians of sub-cell median mixing ratios were used to ensure adequate grid cell coverage of the measurements and reduce the influence of near-source sampling as follows. First, the 4-km CMAQ grid cells were decomposed into 1-km sub-cells, and grid cells with measurements in at least four sub-cells were selected. Second, median NH_3 mixing ratios in each sub-cell were calculated from the 1-s paired model-measurement data. Finally, the median mixing ratio for a 4-km grid cell was calculated as the median of the sub-cell median values. For spatial comparisons of CMAQ predictions and P-3B measurements, mean or median mixing ratios were calculated from the 1-s paired model-measurement data over samples within the modeled PBL during 11-15 PST for grid columns with measurements on at least four days. Modeled PBL heights were well correlated with PBL heights estimated from measurements during P-3B spirals, but predicted values were moderately biased low (12-34%; Figure S2).

3. Results and Discussion

NH_4NO_3 in fine particles is generally considered to be in thermodynamic equilibrium with NH_3 and HNO_3 for time scales of relevance to regional air quality modeling [e.g., *Fountoukis et al.*, 2009; *Meng and Seinfeld*, 1996]. Evaluations of model predictions of NH_3, HNO_3, NOx, and NOy are therefore relevant for understanding the model's ability to simulate NH_4NO_3. In section 3.1, NH_3 predictions are compared with measurements from the mobile ground laboratory and the P-3B aircraft. In section 3.2, predictions of NOx, NOx/NOy, and TNO3 are compared with measurements from the P-3B aircraft. Routine network observations of NO_3^- are also used to understand the model's ability to simulate NO_3^- across the Valley. In section 3.3, the NH_4NO_3 system is considered at the Fresno site where a comprehensive dataset allows for

detailed investigation. Finally, in section 3.4, model predictions of HNO_3 production rates are presented to contribute to understanding of the spatial and temporal patterns of nitrate production in the Valley. The term *NH_4NO_3* is used here for convenience and is not meant to imply a solid phase state. For supersaturated conditions and for stable equilibrium conditions at relative humidities (RHs) greater than the mutual deliquescence RH (MDRH) of the inorganic system, NH_4NO_3 would partially or completely dissociate into NH_4^+ and NO_3^- ions in aqueous solution [e.g., *Kelly et al.*, 2008; *Nenes et al.*, 1998; *Wexler and Seinfeld*, 1991]. Since RH is often high in winter in SJV, CMAQ's assumption that NH_4NO_3 completely dissociates into aqueous solution at all RHs is generally a good one, except possibly during afternoon hours as discussed below.

3.1 Examining NH_3 predictions

Average modeled NH_3 mixing ratios over SJV during 15 January to 5 February 2013 are shown in Figure 1a. Mixing ratios greater than about 7 ppb are predicted throughout SJV, and mixing ratios greater than 20 ppb occur in regions just west of Fresno, around Bakersfield, and a large portion of the eastern side of the Valley between Bakersfield and Fresno. The spatial patterns of elevated NH_3 mixing ratios follow the spatial patterns of NH_3 emissions (Figure 1b) closely. NH_3 emissions occur primarily during daytime (Figure S3a) due to the combination of increased emission-related activity and conducive meteorology [e.g., *Lonsdale et al.*, 2017; *Zhu et al.*, 2015]. On average, NH_3 deposition fluxes in the boxed region of Figure 1b were 43% of the emission fluxes during 10-16 PST, and vertical transport of NH_3 from model layer 1 was 55% of the emission fluxes (Figure S3b). This behavior is consistent with a previous study for the eastern U.S. [*Dennis et al.*, 2010] and explains the correspondence in spatial patterns of NH_3 emissions and model surface layer concentrations in Figure 1.

Model predictions of NH_3 are compared with measurements from the mobile ground laboratory in Figure 2. These comparisons were done by matching CMAQ predictions in space and time with the measurements for all transects and then calculating the median modeled and measured mixing ratio by CMAQ grid cell from median values in 1-km sub-cells as described above. Model predictions are scaled by two in Figure 2a to better illustrate spatial patterns. The model underestimates mixing ratios considerably in regions where elevated values (> ~20 ppb) were measured (Figure 2b). Yet the model correctly estimates that NH_3 mixing ratios are elevated just southwest of Turlock, near Fresno, and in a region to the southeast of Hanford and that NH_3 mixing ratios are relatively low on the western side of the Valley. The model-measurement comparison is complicated by the non-uniform sampling and wide range of scales represented by the high resolution measurements compared with the relatively coarse regional air quality model. The qualitative conclusion of underestimated NH_3 in high emission regions based on the aggregated

results in Figure 2 appears to be robust though based on additional NH_3 evaluation discussed below. Also, previous comparisons of CMAQ predictions with NH_3 measurements in SJV from the NOAA P-3B aircraft during May and June 2010 yielded similar conclusions as here [*Kelly et al.*, 2014]. Model predictions of NO_3^- appear to be insensitive to the NH_3 underpredictions in the high emission regions though. For instance, in a simulation with NH_3 emissions doubled in the boxed region of Figure 1b, average NO_3^- concentrations changed by <5% in 93% of SJV grid cells having NO_3^- concentrations >5 μg m^{-3} and the maximum change was 13%.

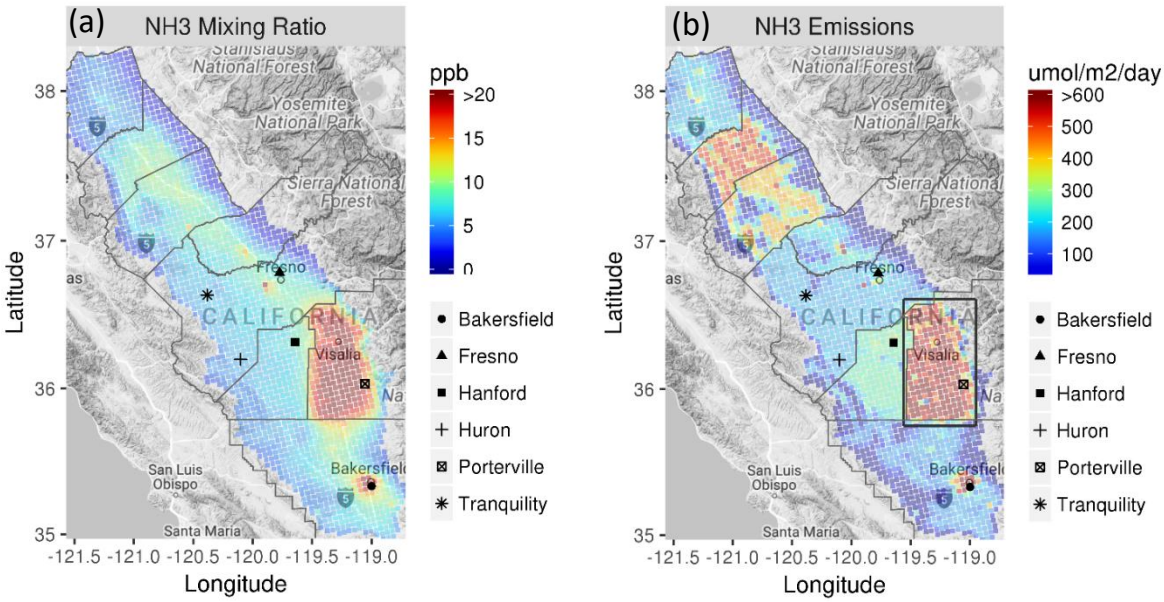

Figure 1. Average NH_3 (a) mixing ratios predicted by CMAQ and (b) gridded emissions during 15 January – 5 February 2013 with county lines, box defining region for discussion, and markers for P-3B spiral locations.

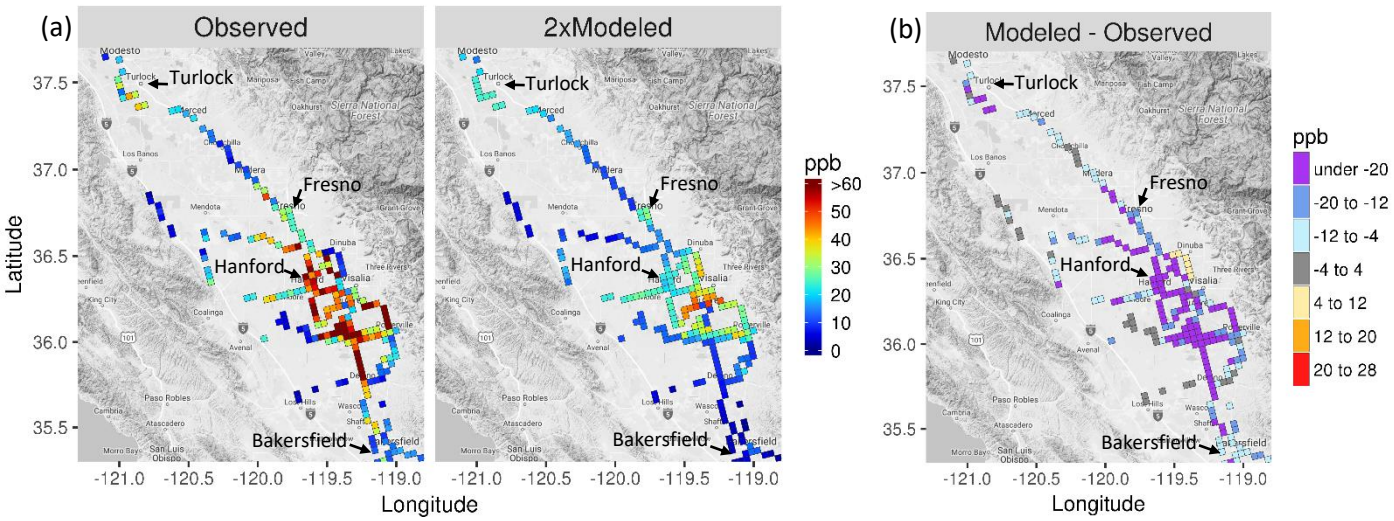

Figure 2. (a) Median observed and 2x median modeled NH_3 mixing ratio by CMAQ grid cell over all mobile ground laboratory sampling transects and (b) difference in median values. See text for description of grid cell median calculations.

Median modeled NH_3 mixing ratios are compared with CRDS and PTR-ToF-MS measurements from the P-3B aircraft in Figure 3. Model results are scaled by three in the figure to better illustrate spatial patterns. Similar to results of the mobile ground laboratory comparison, the spatial patterns of model predictions are in general agreement with P-3B NH_3 measurements, but model predictions are too low in areas where elevated mixing ratios were observed. One location where relatively large underpredictions are evident is Hanford, which is located just outside of the high emission and concentration region in the model (Figure 1). NH_3 measurements from the CRDS and PTR-ToF-MS were in good agreement near the surface during morning and afternoon P-3B aircraft spirals over Hanford (Figure S4) and indicate that median modeled mixing ratios were underpredicted by a factor of 7-9 in the 0-900 m altitude range. For the mobile laboratory comparison in Figure 2, median NH_3 mixing ratios over Hanford were underpredicted by a factor of 5. Considering that Hanford is located just outside of a high emission region in the model, further examination of the spatial allocation of NH_3 emissions in this area is warranted. Modeled PBL heights were in reasonable agreement with empirical estimates at the Hanford site (normalized mean bias: -12%; Figure S2), and so errors in mixing height predictions are unlikely to explain the model-measurement differences.

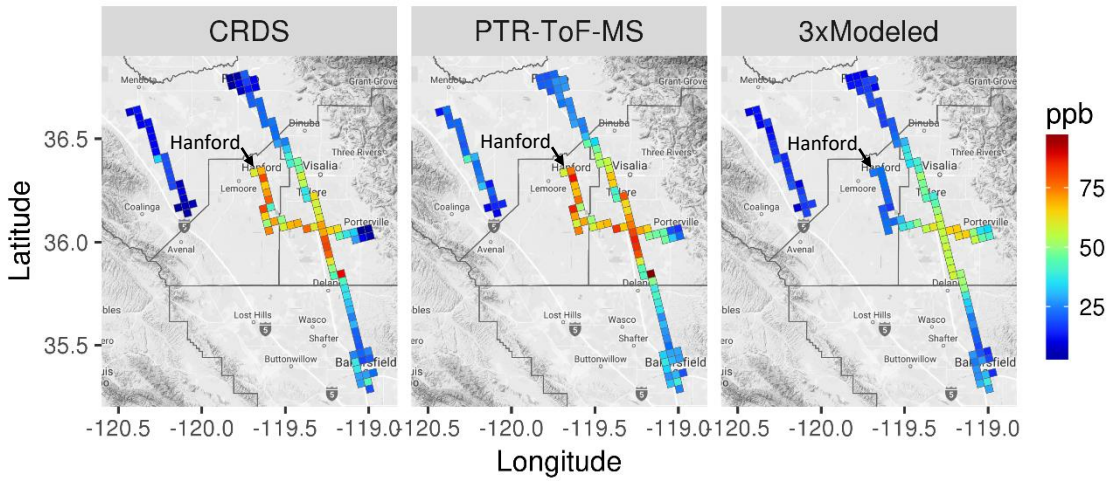

Figure 3. Median modeled and measured NH_3 within the modeled PBL during 11-15 PST by model grid cell for P-3B flights in January and February 2013.

3.2 Examining NOx, NOx/NOy, and NO_3^- predictions

Average model predictions of NOy during 15 January to 5 February are shown in Figure 4a. Relatively high mixing ratios are predicted over Fresno, Bakersfield, and northern SJV cities (e.g., Modesto and Stockton) and along Highway 99 between these cities. Average concentrations of fine particle NO_3^- (Figure 4b) are more uniformly distributed across the Valley than are mixing ratios of NOy, which are elevated in areas with high NOx emissions. The formation of NO_3^- requires the oxidation of NOx to HNO_3 and is promoted by the mixing of urban air masses with air rich in NH_3 from surrounding areas. These dependencies help explain the broader average spatial distributions of NO_3^- than NOy and NH_3 (c.f., Figure 1a). Also, dry deposition velocities of HNO_3 and NH_3 are generally high compared with those of fine particle NO_3^- and contribute to greater spatial gradients in NOy and NH_3.

NOx and NOy were measured during a series of P-3B spirals over sites including major cities in the north (Fresno) and south (Bakersfield), rural locations in the west (Tranquility and Huron), and the Hanford site discussed above. In Figure 5a, model predictions of NOx are compared with measurements during the aircraft spirals. The model correctly predicted that the highest mixing ratios occurred in Bakersfield and Fresno, relatively low mixing ratios occurred in Tranquility and Huron, and mixing ratios generally decreased with altitude. Yet NOx predictions were biased high in the 0-300 m bin at Bakersfield, Fresno, and Tranquility. The ratios of NOx-to-NOy are shown in Figure 5b, where modeled NOy was calculated by summing gas-phase NOy components and 20% of fine particle NO_3^-. Size distribution measurements during the flights indicate that the majority of fine particle NO_3^- existed in particles with diameters less than 500

nm (Figure S5) and suggest that a significant, although unknown, fraction of fine particle NO_3^- was measured by the NOy instrument. NOx-to-NOy ratio comparisons based on modeled NOy with 0% and 100% of modeled NO_3^- included in the NOy calculation are provided in Figure S6. The model captured the general pattern of relatively high NOx-to-NOy ratios in urban areas (e.g., Bakersfield), where fresh NOx emissions comprise a large fraction of NOy, and relatively low NOx-to-NOy ratios in remote areas (e.g., Huron), where NOx oxidation products comprise a large fraction of NOy (Figure 5b). The model also captured the generally decreasing trends of NOx-to-NOy ratios with altitude. The overestimates of the NOx-to-NOy ratios in Fresno, Bakersfield, and Tranquility in Figure 5b suggest that the overpredictions of NOx in Figure 5a could be due in part to too-low modeled oxidation rates. However, the NOx-to-NOy evaluation is limited by uncertainty in the fraction of particle NO_3^- measured by the NOy instrument. Underpredictions of HCHO and O_3 during the aircraft spirals suggest that modeled oxidation rates may have been too low over the sites (Figure S7).

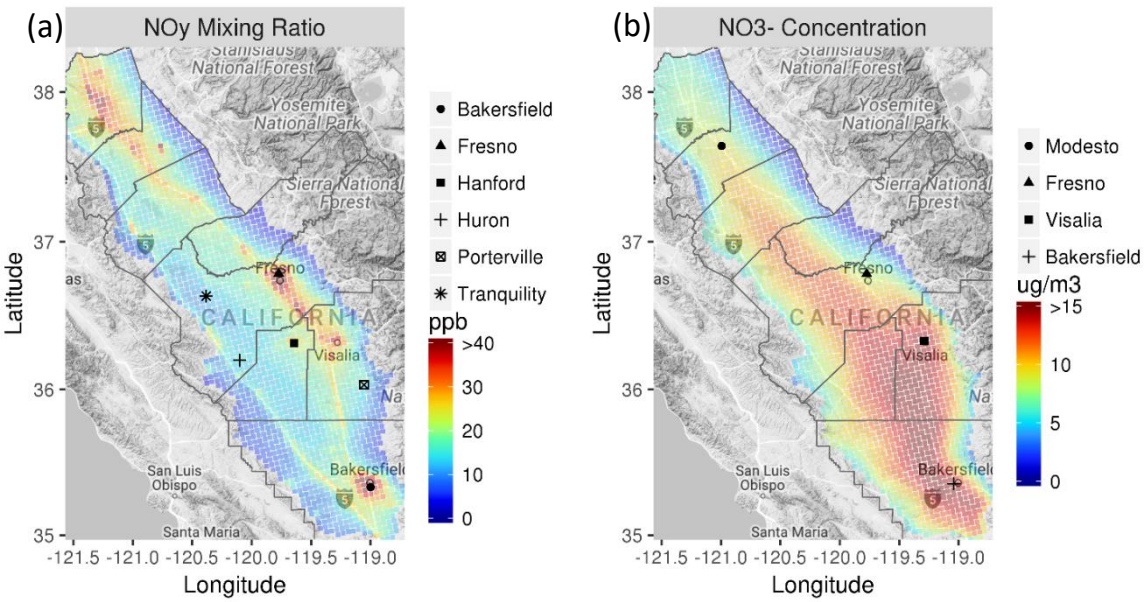

Figure 4. Average (a) NOy (including fine particle NO_3^-) mixing ratios predicted in SJV with markers for P-3B spiral locations and (b) fine particle NO_3^- concentrations with markers for $PM_{2.5}$ monitoring locations during 15 January – 5 February 2013.

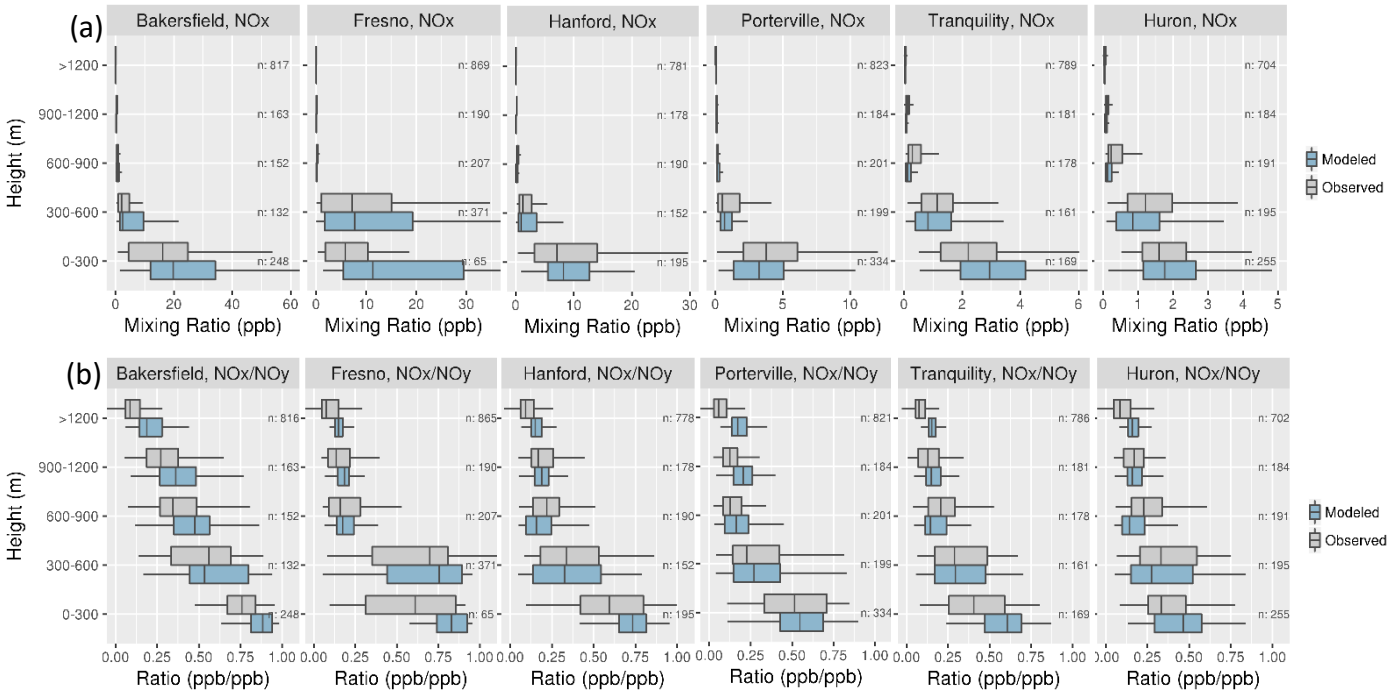

Figure 5. Comparison of modeled and measured (a) NOy and (b) NOx/NOy mixing ratio distributions for 300-m altitude ranges for P-3B aircraft spirals (see Figure 4a for site locations). Boxes bracket the interquartile range (IQR), lines within the boxes represent the median, and whiskers represent 1.5 times the IQR from either end of the box.

In Figure 6, average TNO3 mixing ratios are shown for P-3B measurements at altitudes within the modeled PBL during 11-15 PST by model grid cell for cells with measurements on at least four days. Modeled TNO3 mixing ratios were generally biased high compared with the measurements, especially along Highway 99 between Fresno and Bakersfield. The relatively large TNO3 overpredictions between Bakersfield and Fresno resulted in weaker daytime gradients between the cities and surrounding areas for the model than were identified by *Pusede et al.* [2016]. Modeled TNO3 was biased low relative to the ground site measurements in Fresno (see section 3.3).

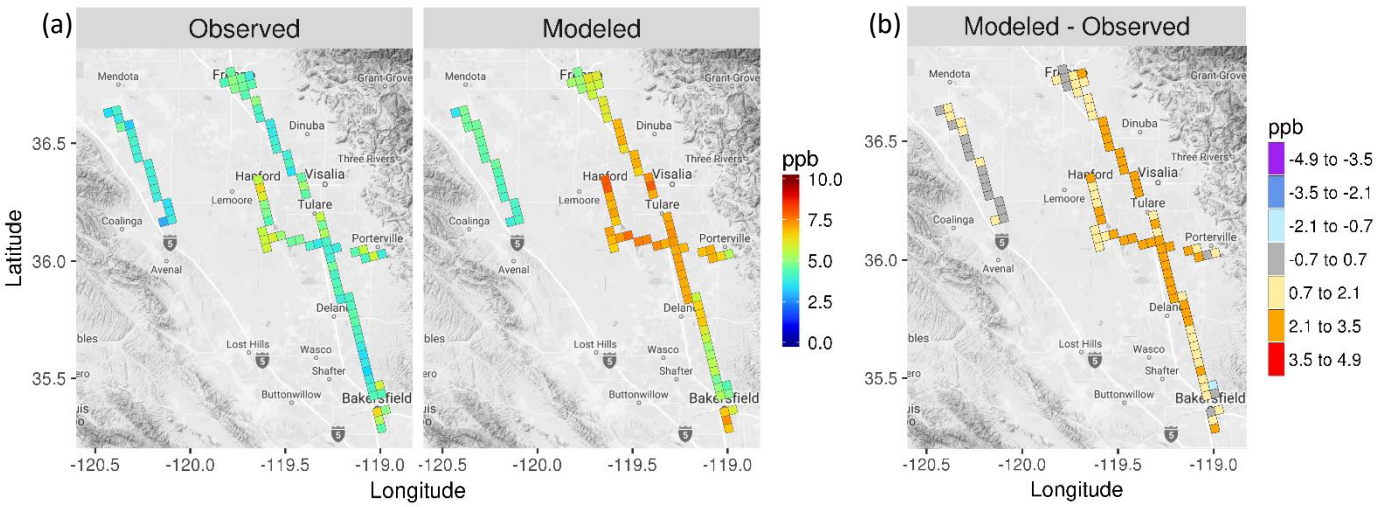

Figure 6. (a) Average modeled and measured TNO3 within the modeled PBL by model grid cell over P-3B flights in January and February 2013 and (b) difference between modeled and measured TNO3.

In Figure 7, model predictions are compared with routine observations of 24-h average fine particle NO_3^- at four sites spanning SJV from north (Modesto) to south (Bakersfield) (see Figure 4b for site locations). A peak in the NO_3^- time series was observed at all sites on January 22nd. The model performed well on this day for all sites except Bakersfield for which observations were underpredicted. On February 3, high NO_3^- concentrations (>20 μg m^{-3}) were observed in the south (Bakersfield and Visalia) and lower concentrations (<10 μg m^{-3}) were observed in the north (Modesto and Fresno). The model underpredicted the NO_3^- peaks on February 3 at Bakersfield and Visalia. The root-mean-square error (RMSE) for predictions increased in magnitude from north (1 μg m^{-3}) to south (7 μg m^{-3}), whereas correlation coefficients were high ($r \geq 0.78$) at all sites.

The mean modeled PBL height at 15 PST was 320 m during the 18-22 January period when elevated NO_3^- was simulated in Modesto and Fresno and was 490 m during the 1-5 February period when the model predicted lower NO_3^- concentrations (Figure S8). Wind speeds were also lower during the January period (mean: 1.4 m/s) than the February period (mean: 1.9 m/s). Compared with profiler measurements at Visalia, wind speeds were biased low in mid-January and were biased high near the surface in early February (Table S1). Considering that meteorological stagnation is central to the conceptual model of NO_3^- formation and build-up in SJV, the relatively low NO_3^- concentrations simulated during the early February period are probably related to the greater transport and mixing in the model. The relatively large NO_3^- underpredictions at Bakersfield, where meteorology is more influenced by the convergence of mountain ranges to the south, may be attributed to challenges in simulating meteorology in complex terrain.

However, a full evaluation of the three-dimensional meteorological fields across the Valley and their impact on air quality during these periods is not straightforward and is beyond the scope of this study.

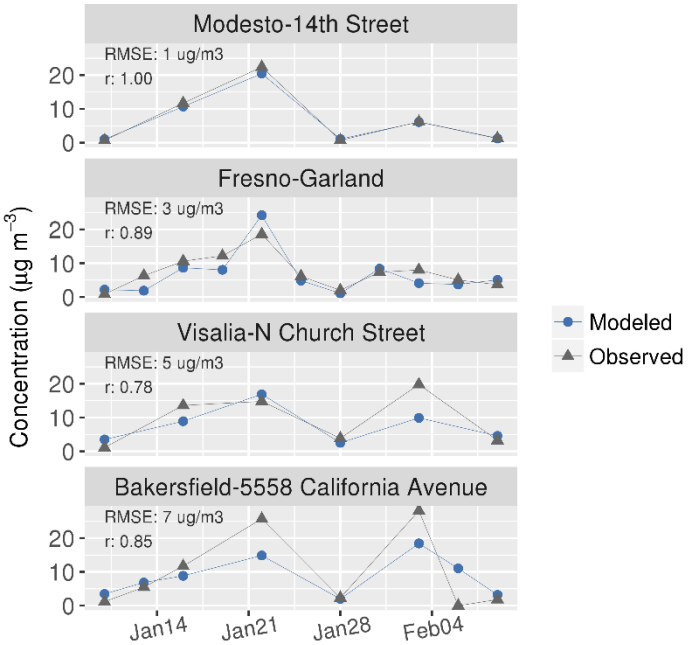

Figure 7. Comparison of 24-h average $PM_{2.5}$ NO_3^- predictions of CMAQ with routine monitoring measurements at sites shown in Figure 4b.

3.3 Examining the NH_4NO_3 system in Fresno

A relatively complete set of measurements for evaluating the NH_4NO_3 system were made during 19 January – 10 February 2013 at the CARB Fresno-Garland site. In Figure 8, predictions of fine particle NO_3^- are compared with PILS-IC measurements at this site. Two major NO_3^- episodes were identified in Fresno during the campaign from about 14-23 January and 29 January to 5 February [*Young et al.*, 2016]. During the first episode, the model overpredicted the peak NO_3^- concentration on 22 January (Figure 8). The modeled peak is due to overnight transport of NO_3^- from the south (Figure S10), where modeled production of HNO_3 was particularly high around Visalia during this period (see section 3.4). Modeled wind speeds were low in Visalia in reasonable agreement with observations (Figure S11–S13). However, observed winds at sites in SJV were relatively disorganized overnight compared with model predictions and suggest that the model overestimated transport of NO_3^- to Fresno on January 22. In early February, the model underpredicted the elevated NO_3^- concentrations in Fresno. As discussed above, modeled wind speeds and PBL heights were relatively high across SJV during the February period, and modeled NO_3^- concentrations

were relatively low. Comparisons of predictions of SO_4^{2-}, NH_4^+, K^+, and Cl^- with PILS-IC measurements are provided in Figure S14. Underpredictions of the generally modest measured Cl^- concentrations are consistent with findings of studies of other parts of the U.S. [*Kelly et al.*, 2016; *Kelly et al.*, 2014; *Kelly et al.*, 2010; *Simon et al.*, 2010].

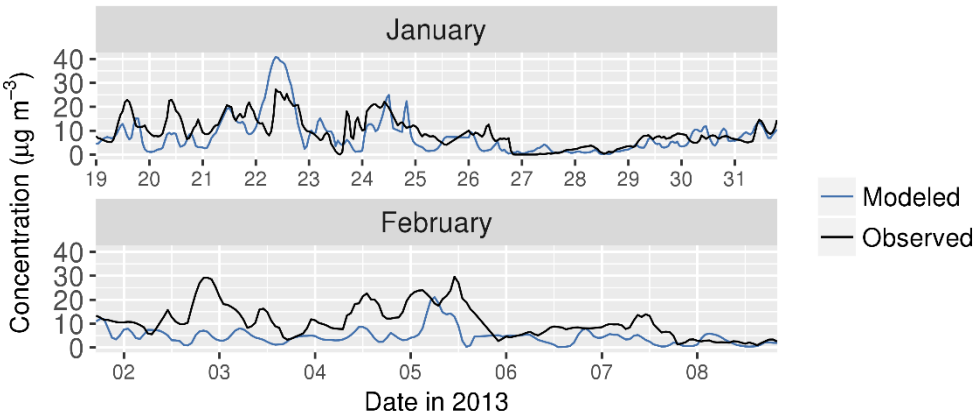

Figure 8. Comparison of model predictions of fine particle NO_3^- with PILS-IC measurements at the Fresno-Garland ground site.

Distributions of hourly average modeled and measured NO_3^- concentrations in Fresno are shown in Figure 9 for the January and February episodes. Measured concentrations increase in the morning during both periods in a pattern consistent with mixing of NH_4NO_3 from the nocturnal residual layer to the surface during development of the daytime boundary layer [*Parworth et al.*, 2017; *Prabhakar et al.*, 2017; *Young et al.*, 2016]. The 75th percentiles of modeled concentrations increase in the morning during the 19-25 January episode, but median concentrations are relatively constant compared with the measurements. The morning increase in NO_3^- is also underpredicted during 30 January - 5 February. In the afternoon, measured NO_3^- concentrations reach a relatively constant level during the first period and decrease during the second period, whereas modeled concentrations decrease in the afternoon during both episodes (Figure 9).

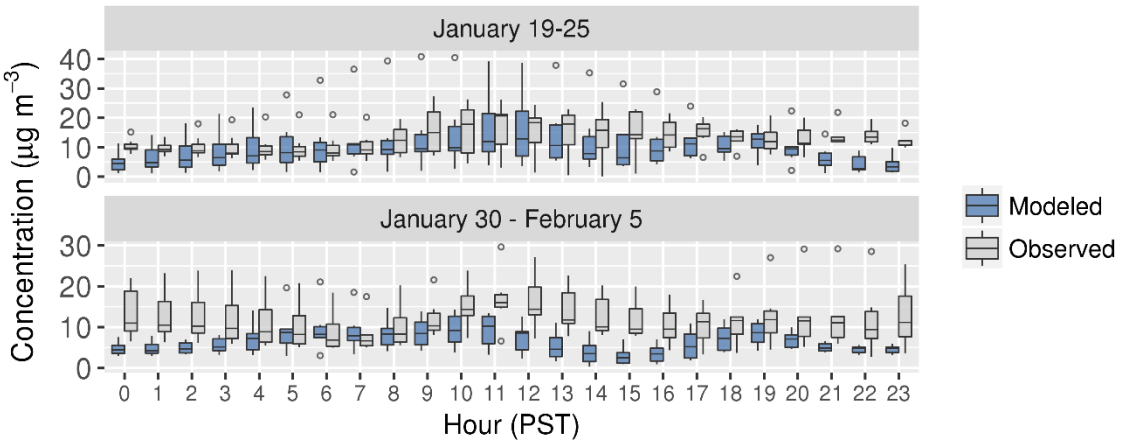

Figure 9. Hourly average modeled and measured NO_3^- distributions at Fresno ground site during two periods of interest. Boxes bracket the IQR, lines within the boxes represent the median, whiskers represent 1.5 times the IQR from either end of the box, and circles represent individual values less than and greater than the range of the whiskers.

In Figure 10, concentrations of TNO3 and NHx and the percentage of the total concentrations in the gas phase are shown during 19-31 January when model performance for NO_3^- was relatively good. The model is biased 27% low for TNO3 and 36% low for NHx during this period at the Fresno site. However, the model correctly predicts that most of NHx is in the gas phase and most of TNO3 is in the particle phase. This gas-particle partitioning behavior suggests that HNO_3 is the limiting precursor for NH_4NO_3 formation in SJV in both the model and ambient. Sensitivity simulations with reductions in NH_3 and NOx emissions were conducted and confirmed that HNO_3 is the limiting precursor in the model.

Although gas-particle partitioning is generally predicted well, the fraction of TNO3 in the gas phase is sometimes overestimated in the model (Figure 10b). The overestimates of partitioning to the gas phase appear to be driven primarily by meteorology (i.e., RH and temperature, T) rather than issues with particle composition predictions. The modeled gas-phase fraction of TNO3 is relatively high when RH is less than 50% and T is greater than 285 K (Figure S15a). The overpredictions of the gas-phase fraction of TNO3 under these conditions could be due in part to challenges in representing the particle phase state under low RH conditions. Recall that the model assumes crystallization does not occur and inorganic components exist as ions in supersaturated solutions for low RH (e.g., RH<MDRH). Previous studies have found that this assumption yields lower predicted NO_3^- concentrations compared with the stable equilibrium assumption for RH < ~50% [*Ansari and Pandis*, 2000; *Fountoukis et al.*, 2009]. To investigate the issue here, offline simulations with ISORROPIA II were performed for cases of stable (i.e., including crystallization) and metastable (i.e., no crystallization) equilibrium using T, RH, and concentration inputs based on CMAQ

output for hours where the sampling period average RH was <50%. These simulations confirmed that the phase state assumption influences partitioning predictions under the low-RH conditions in Fresno. For hours with RH between 37% and 54%, the average percentage of TNO3 in the gas phase was 50% for simulations based on the metastable assumption and 24% for the stable assumption. Segregation of results by time of day (Figure S15b) reveals that the overpredictions of partitioning of TNO3 to the gas phase occur in the afternoon. The overestimate of the decreasing trend in NO_3^- concentration in the afternoon in the top panel of Figure 9 could therefore be due in part to gas-particle partitioning prediction issues, which are sensitive to particle phase state assumptions under low RH conditions. Deposition rates of TNO3 are relatively large in the afternoon due to the relatively low atmospheric resistance of the convective boundary layer (Figure S16). The average modeled deposition velocity was 2.83 cm s^{-1} for HNO_3 and 0.07 cm s^{-1} for accumulation mode particles during 12-17 PST, 19-31 January. Given the relatively high deposition velocity of HNO_3 compared with that of fine particle NO_3^-, excessive partitioning of TNO3 to the gas phase could lead to excessive removal of TNO3 through HNO_3 dry deposition in the afternoon.

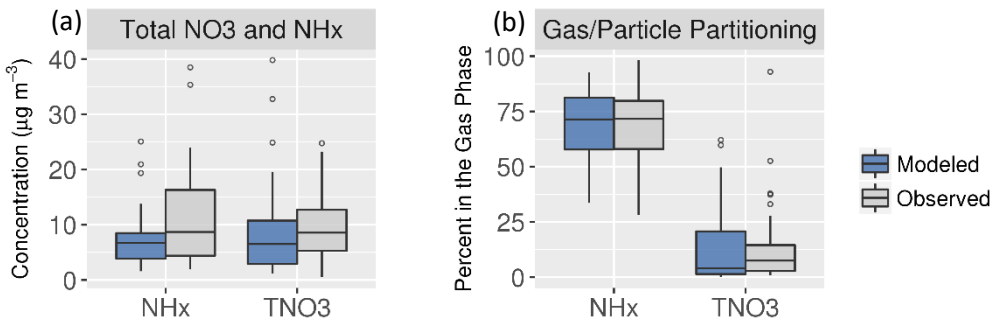

Figure 10. Modeled and measured concentrations of (a) TNO3 and NHx and (b) percentage of total in the gas phase during 19 – 31 January at the Fresno ground site.

3.4 Examining HNO_3 production

Previous studies and the current modeling indicate that the limiting precursor for NH_4NO_3 formation in SJV is HNO_3. Understanding chemical production of HNO_3 is therefore important for understanding NH_4NO_3 formation. HNO_3 production during daytime when OH levels are high is typically dominated by R1:

$$NO_2 + OH \rightarrow HNO_3. \qquad (R1)$$

At night, when OH mixing ratios are low and photolysis of NO_3 radical is negligible, heterogeneous hydrolysis of gas-phase N_2O_5 with particle-phase H_2O (R2) is important

458 $N_2O_5 + H_2O(p) + Y\ Cl^-(p) \rightarrow Y(HNO_3 + ClNO_2) + 2\ (1\text{-}Y)\ HNO_3$ (R2)

459 where Y is the yield of $ClNO_2$ [*Bertram and Thornton*, 2009; *Roberts et al.*, 2009]. O_3 is an important oxidant
460 in the production of N_2O_5 at night:

461 $NO + O_3 \rightarrow NO_2 + O_2$ (R3)

462 $NO_2 + O_3 \rightarrow NO_3$ (R4)

463 $NO_2 + NO_3 \leftrightarrow N_2O_5$. (R5)

464 Hourly 75th percentile HNO_3 production rates for R1, R2, homogeneous hydrolysis of N_2O_5 with water
465 vapor, and heterogeneous hydrolysis of organic nitrates over Fresno are shown in Figure 11a for model
466 layer 1, 5, and 7 during 17-22 January. Reaction of NO_2 with OH (R1) dominates HNO_3 production in all
467 layers during daytime. Overnight, heterogeneous N_2O_5 hydrolysis (R2) dominates production in layer 5 and
468 7. This HNO_3 can condense to form fine particle NO_3^- and increase surface NO_3^- concentrations in the
469 morning as the daytime boundary layer develops (e.g., Figure 9). In the surface layer overnight, R1 and R2
470 contribute similarly to HNO_3 production over Fresno in the model. OH mixing ratios that drive R1 are
471 typically low at night because photolysis reactions important for OH production are negligible. The primary
472 source of OH in the model at night is the reaction $NO + HO_2 \rightarrow OH + NO_2$. This reaction is important in the
473 model surface layer over Fresno because of the substantial NO emissions and the limited vertical mixing at
474 night. HO_2 sources in the model that do not directly depend on sunlight include reactions of organics with
475 O_3 and NO. Measured increases in surface NO_3^- concentrations in Fresno in the morning suggest that
476 production in the ambient surface layer over Fresno is relatively small compared with production aloft.
477 Therefore, there is evidence that HNO_3 production in the nighttime surface layer over Fresno is too high.
478 Also, O_3 mixing ratios in the surface layer are overestimated at the Fresno site overnight during this period
479 (Figure S17a). Observations indicate that O_3 is almost entirely depleted at the site on most nights due to
480 the high NOx levels and reactions such as R3 and R4. NOx mixing ratios are lower in the model than the
481 ambient overnight and enable partial recovery of O_3 mixing ratios following decreases during the evening
482 rush hour when NOx emissions are high.

483 The apparently excessive production of HNO_3 in the model surface layer over Fresno at night appears to
484 be due to overpredictions of O_3 mixing ratios. The cause of high O_3 mixing ratios in the surface layer in the
485 model is vertical transport from higher layers. To test the impact of vertical mixing at night on the
486 production of HNO_3 over Fresno, a sensitivity simulation was conducted where CMAQ's parameterization
487 for the minimum eddy diffusivity ($K_{z,min}$) was replaced by a fixed $K_{z,min}$ of 0.01 $m^2\ s^{-1}$ in all grid cells as is done

in ACM2 in the WRF model. The $K_{z,min}$ change reduced vertical mixing of species overnight over Fresno, because ACM2 in CMAQ uses higher $K_{z,min}$ values in urban areas [*USEPA*, 2012a]. O_3 depletion in the surface layer was nearly complete overnight during 17-22 January in the simulation with reduced vertical mixing (Figure S17b), and HNO_3 production in the surface layer was significantly reduced compared with the base simulation (Figure 11b). However, the underestimate of the morning increase in NO_3^- was not resolved by reducing $K_{z,min}$. Advection of the nocturnal residual layer from Fresno to the south likely contributed to the underestimate of the morning increase in NO_3^- in the model. In a simulation with increased CO emissions in Fresno grid cells, the largest impacts on CO mixing ratios aloft at night were to the south of Fresno during this period (Figure S18).

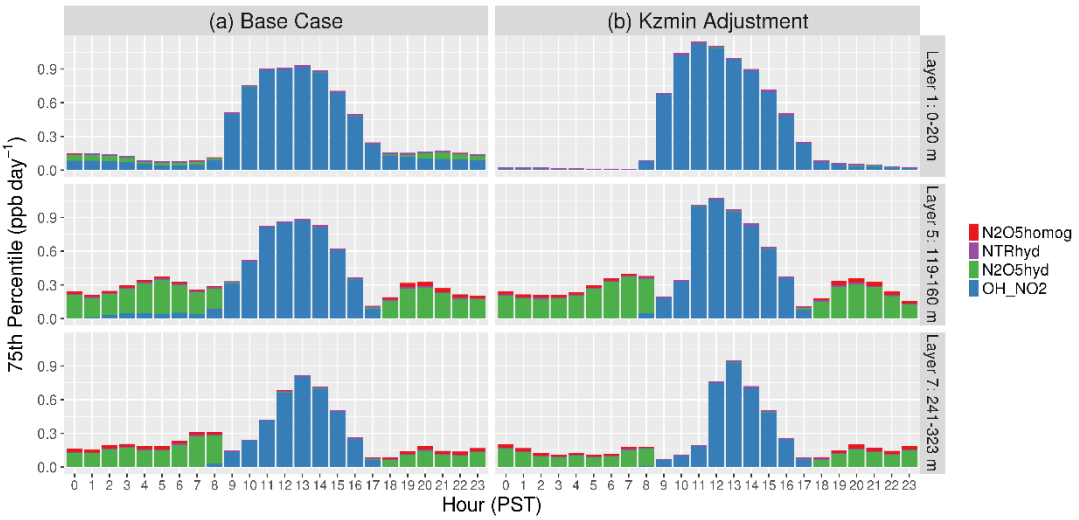

Figure 11. Hourly 75th percentile HNO_3 production rates by chemical pathway over Fresno for the (a) base simulation and (b) simulation with $K_{z,min}$=0.01 m^2 s^{-1} during January 17 – 22. N2O5homog: homogeneous gas phase reaction of N_2O_5 + H_2O; NTRhyd: heterogeneous hydrolysis of organic nitrates; N2O5hyd: heterogeneous hydrolysis of N_2O_5; and OH_NO2: reaction of OH+NO_2.

HNO_3 production integrated over model layers 1-20 is shown in Figure 12a for SJV grid cells during 17-22 January. R1 is the dominant production pathway in urban areas with large NOx emissions such as Fresno and Bakersfield in the model. The R2 pathway is dominant in semi-urban and rural areas along Highway 99, particularly around Visalia and in northern SJV. HNO_3 production in SJV peaks in model layer 6 (160 - 240 m; Figure 12c). R1 is productive in the middle of the daytime boundary layer due to the combination of relatively high OH and NO_2, and R2 tends to be most productive in the nocturnal residual layer due to the combination of high N_2O_5 and aerosol surface area [*Riemer et al.*, 2003]. Overall, the model estimates that R1 contributes 46% and R2 contributes 54% to total HNO_3 production for the 17-22

January period when the model predicted elevated NO_3^-. This apportionment is similar to model estimates from previous episodes [*Ying and Kleeman*, 2009]. In early February, when the model under-predicted NO_3^- concentrations, the modeled boundary layer was deeper during the day and production occurred over a wider range of altitudes (Figure 12d). The R2 pathway was relatively weak in the model in the area between Fresno and Bakersfield in early February (Figure 12b) compared with 17-22 January (Figure 12a).

Pusede et al. [2016] predicted that HNO_3 production from R1 would increase relative to R2 with decreasing NOx emissions. To explore the sensitivity of HNO_3 production to NOx levels in the model, a sensitivity simulation was conducted with NOx emissions reduced by 40%. In this simulation, R1 contributed 49% to integrated HNO_3 production during 17-22 January (i.e., production from R1 was enhanced relative to R2 compared with the base simulation). Decreases in NOx emissions lead to increases in OH mixing ratios in urban areas and along major highways in the model and thereby increase the percent contribution of R1 to total HNO_3 production relative to that of the base simulation. This behavior is qualitatively consistent with predictions of *Pusede et al.* [2016], although that study focused on the entire winter period rather than the multiday episode considered here. A wide range of N_2O_5 heterogeneous reaction probabilities (i.e., the fraction of gas-particle collisions that result in net removal of N_2O_5 from the gas phase, γ) have been used in previous studies of NO_3^- formation in SJV [e.g., *Prabhakar et al.*, 2017; *Ying and Kleeman*, 2009]. To explore the sensitivity of HNO_3 production to γ and the $ClNO_2$ yield (Y in R2), three additional simulations were conducted with γ scaled by 0.5 and 1.5 and with Y=0. Total HNO_3 production decreased by 11% relative to the base case when γ was reduced by 50% for the scenario in Figure 12a. A 24% reduction in HNO_3 production from R2 was partially compensated for by a 5% increase in production from R1. Total HNO_3 production increased by 6% relative to the base case in the simulation with a 50% increase in γ. Setting the yield of $ClNO_2$ to zero had negligible impact on HNO_3 production consistent with the generally low concentrations of Cl^- in SJV, although Cl^- was underpredicted (Figure S14). γ values predicted over the P-3B spiral sites during 17-22 January are shown in Figure S19.

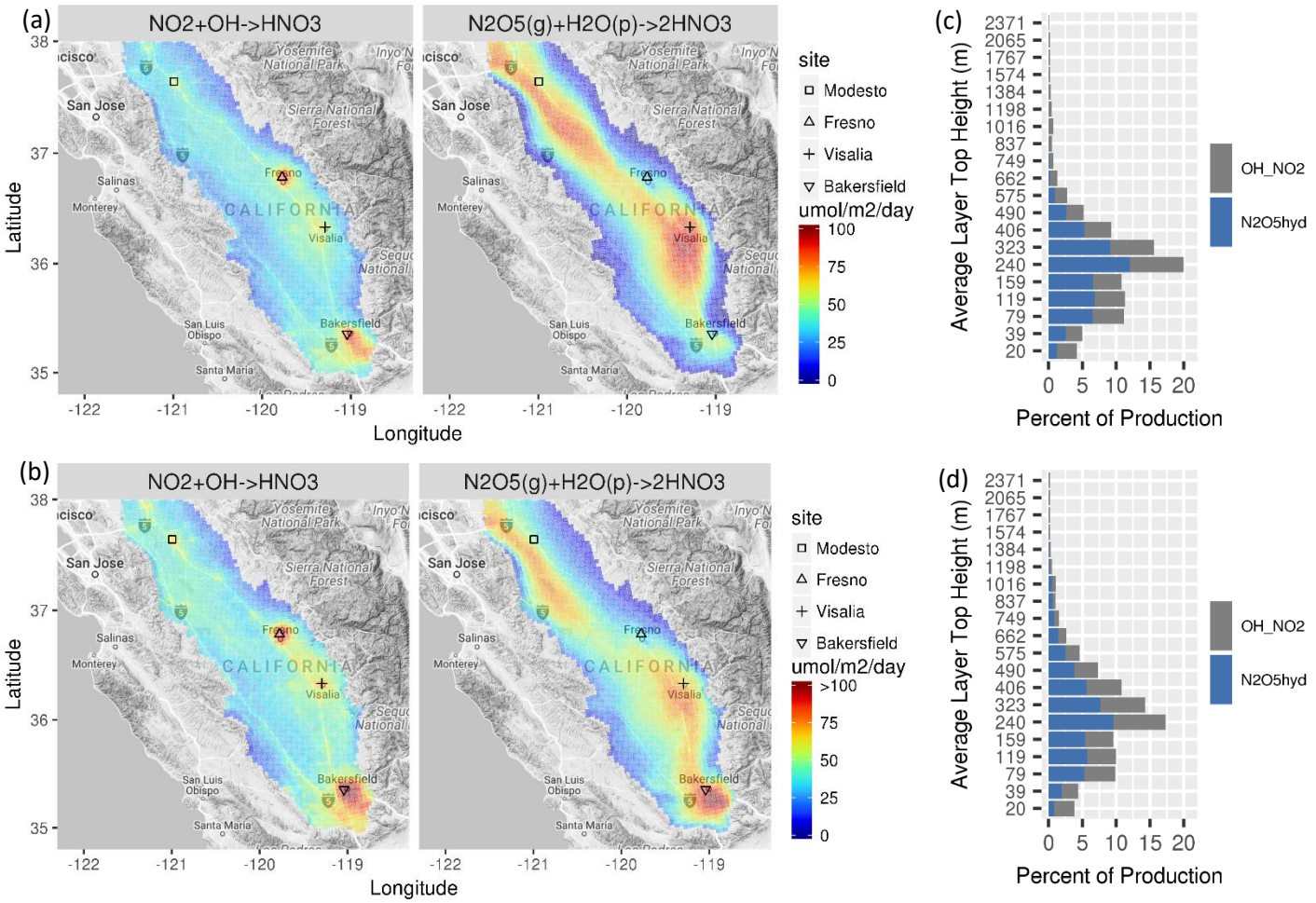

Figure 12. HNO_3 production integrated over layers 1-20 for SJV model grid cells during (a) 17-22 January and (b) 29 January - 4 February and integrated over SJV grid cells by model layer during (c) 17-22 January and (d) 29 January - 4 February.

4. Conclusions

This study demonstrates that regional photochemical grid models are capable of simulating NH_4NO_3 formation and build-up during major recent $PM_{2.5}$ episodes in SJV. For example, routine measurements of NO_3^- were generally predicted well at sites in SJV, including days where 24-h average NO_3^- reached 20 μg m^{-3}. Gas-particle partitioning predictions were in good agreement with measurements in Fresno and indicate that the model correctly predicts that NH_4NO_3 formation is limited by HNO_3 availability. Modeled chemical production of HNO_3 via daytime and nighttime pathways was generally consistent with reports from previous studies and conceptual models of NO_3^- formation in SJV. During a period of elevated NH_4NO_3, the

549 model predicted that the OH + NO_2 pathway contributed 46% to total HNO_3 production in SJV and the N_2O_5
550 heterogeneous hydrolysis pathway contributed 54%.

551 Despite generally favorable model performance, the 2013 SJV DISCOVER-AQ dataset provided insights
552 on areas where additional work could improve NH_4NO_3 modeling for SJV. First, additional study on
553 meteorological modeling of the major stagnation events that drive $PM_{2.5}$ episodes in the Valley would be
554 valuable, particularly for southern SJV where the terrain is more complex than in central and northern SJV.
555 Challenges in simulating meteorology in southern SJV could help explain the better NH_4NO_3 model
556 performance for Fresno and Modesto than Bakersfield. Also, work toward improving the simulation of
557 diurnal patterns of vertical mixing would be valuable, because the coupling and decoupling of processes in
558 the surface layer from layers aloft influences HNO_3 production and the diurnal profiles of NH_4NO_3 at the
559 surface. Additional evaluation of the degree to which urban-nonurban transport of NO_3^- occurs in the
560 ambient would also be helpful because predictions suggest that this transport can be important.
561 Improvements in meteorological modeling are likely necessary to improve performance against the hourly
562 average NO_3^- measurements in Fresno. Second, additional work on NH_3 modeling is warranted based on
563 underpredictions of NH_3 in emission source regions where very high mixing ratios were measured.
564 Although the NH_3 underpredictions do not appear to have a large impact on NO_3^- predications (because
565 NO_3^- is HNO_3-limited), NH_3 levels are too low in the model in source regions and warrant further study.
566 Improvements in the spatial allocation of NH_3 emissions near Hanford and elsewhere are also warranted.
567 Third, there is evidence that gas-particle partitioning predictions under low-RH conditions could benefit
568 from additional study. Although the overall impact of gas-particle partitioning issues may be minor due to
569 the generally high RH during SJV $PM_{2.5}$ episodes, the potential for premature removal of TNO3 via rapid
570 deposition of HNO_3 when the gas-phase fraction is overestimated in afternoon makes this an area of
571 interest.

572 Another topic for future investigation is on HNO_3 production in the nocturnal residual layer over urban
573 and surrounding areas. Although this pathway is central to the conceptual model of NO_3^- formation in SJV,
574 measurements that can directly constrain nighttime HNO_3 production aloft over SJV are extremely limited.
575 Researchers have made progress by using indirect methods to infer characteristics of the nocturnal residual
576 layer based on measurements over urban areas on the previous day and following morning, but direct
577 measurements of the key species at night over urban and surrounding areas would be valuable.

578

579 Acknowledgments

The authors recognize contributions from Ellen Cooter, Rob Gilliam, Deborah Luecken, Limei Ran, Golam Sarwar, Chris Allen, Allan Beidler, James Beidler, and Lara Reynolds.

Disclaimer

Although this work was reviewed by EPA and approved for publication, it may not necessarily reflect official Agency policy.

References

Ansari, A. S., and S. N. Pandis (2000), The effect of metastable equilibrium states on the partitioning of nitrate between the gas and aerosol phases, *Atmospheric Environment*, *34*(1), 157-168, doi:http://dx.doi.org/10.1016/S1352-2310(99)00242-3.

Appel, K. W., et al. (2017), Description and evaluation of the Community Multiscale Air Quality (CMAQ) modeling system version 5.1, *Geoscientific Model Development*, *10*(4), 1703-1732, doi:10.5194/gmd-10-1703-2017.

Bash, J. O., K. R. Baker, and M. R. Beaver (2016), Evaluation of improved land use and canopy representation in BEIS v3.61 with biogenic VOC measurements in California, *Geosci. Model Dev.*, *9*(6), 2191-2207, doi:10.5194/gmd-9-2191-2016.

Bash, J. O., E. J. Cooter, R. L. Dennis, J. T. Walker, and J. E. Pleim (2013), Evaluation of a regional air-quality model with bidirectional NH3 exchange coupled to an agroecosystem model, *Biogeosciences*, *10*(3), 1635-1645, doi:10.5194/bg-10-1635-2013.

Bertram, T. H., and J. A. Thornton (2009), Toward a general parameterization of N2O5 reactivity on aqueous particles: the competing effects of particle liquid water, nitrate and chloride, *Atmospheric Chemistry and Physics*, *9*(21), 8351-8363.

Blanchard, C. L., P. M. Roth, S. J. Tanenbaum, S. D. Ziman, and J. H. Seinfeld (2000), The Use of Ambient Measurements To Identify which Precursor Species Limit Aerosol Nitrate Formation, *Journal of the Air & Waste Management Association*, *50*(12), 2073-2084, doi:10.1080/10473289.2000.10464239.

CDFA (2016a), California Department of Food and Agriculture, California Agricultural Statistics Review 2015-2016, *Available: https://www.cdfa.ca.gov/statistics/PDFs/2016Report.pdf*.

CDFA (2016b), California Department of Food and Agriculture, Dairy Statistics: 2016 Annual Data, *Available: https://www.cdfa.ca.gov/dairy/pdf/Annual/2016/2016_Statistics_Annual.pdf*.

CDOC (2015), California Department of Conservation, Division of Oil, Gas, & Geothermal Resources, 2015: Well Count and Oil and Gas Production by County, *Retrieved from http://www.conservation.ca.gov/dog*.

CDOF (2017), Calfornia Department of Finance, Press Release: Department of Finance Releases New State Population Projections, *Available: http://www.dof.ca.gov/Forecasting/Demographics/projections/documents/P_PressRelease.pdf*

614 Chen, J., J. Lu, J. C. Avise, J. A. DaMassa, M. J. Kleeman, and A. P. Kaduwela (2014), Seasonal modeling of
615 PM2.5 in California's San Joaquin Valley, *Atmospheric Environment*, *92*, 182-190,
616 doi:http://dx.doi.org/10.1016/j.atmosenv.2014.04.030.

617 Chen, J., Q. Ying, and M. J. Kleeman (2009), Source apportionment of visual impairment during the
618 California regional PM10/PM2.5 air quality study, *Atmospheric Environment*, *43*(39), 6136-6144,
619 doi:http://dx.doi.org/10.1016/j.atmosenv.2009.09.010.

620 Chen, J., Q. Ying, and M. J. Kleeman (2010), Source apportionment of wintertime secondary organic aerosol
621 during the California regional PM10/PM2.5 air quality study, *Atmospheric Environment*, *44*(10), 1331-1340,
622 doi:http://dx.doi.org/10.1016/j.atmosenv.2009.07.010.

623 Chen, L. W. A., J. G. Watson, J. C. Chow, and K. L. Magliano (2007), Quantifying PM2.5 source contributions
624 for the San Joaquin Valley with multivariate receptor models, *Environmental Science & Technology*, *41*(8),
625 2818-2826, doi:10.1021/es0225105.

626 Chow, J. C., L. W. A. Chen, J. G. Watson, D. H. Lowenthal, K. A. Magliano, K. Turkiewicz, and D. E. Lehrman
627 (2006), PM2.5 chemical composition and spatiotemporal variability during the California Regional
628 PM10/PM2.5 Air Quality Study (CRPAQS), *Journal of Geophysical Research-Atmospheres*, *111*(D10),
629 doi:10.1029/2005jd006457.

630 Collett, J. L., K. J. Hoag, and X. Rao (1999a), Internal acid buffering in San Joaquin Valley fog drops and its
631 influence on aerosol processing, *Atmospheric Environment*, *33*(29), 4833-4847, doi:10.1016/s1352-
632 2310(99)00221-6.

633 Collett, J. L., K. J. Hoag, D. E. Sherman, A. Bator, and L. W. Richards (1999b), Spatial and temporal variations
634 in San Joaquin Valley fog chemistry, *Atmospheric Environment*, *33*(1), 129-140.

635 Davis, J. M., P. V. Bhave, and K. M. Foley (2008), Parameterization of N2O5 reaction probabilities on the
636 surface of particles containing ammonium, sulfate, and nitrate, *Atmos. Chem. Phys.*, *8*(17), 5295-5311,
637 doi:10.5194/acp-8-5295-2008.

638 Dennis, R. L., R. Mathur, J. E. Pleim, and J. T. Walker (2010), Fate of ammonia emissions at the local to
639 regional scale as simulated by the Community Multiscale Air Quality model, *Atmospheric Pollution*
640 *Research*, *1*(4), 207-214, doi:http://dx.doi.org/10.5094/APR.2010.027.

641 Fountoukis, C., and A. Nenes (2007), ISORROPIA II: a computationally efficient thermodynamic equilibrium
642 model for K+-Ca2+-Mg2+-NH4+-Na+-SO42--NO3-Cl--H2O aerosols, *Atmos. Chem. Phys.*, *7*(17), 4639-4659,
643 doi:10.5194/acp-7-4639-2007.

644 Fountoukis, C., A. Nenes, A. Sullivan, R. Weber, T. Van Reken, M. Fischer, E. Matías, M. Moya, D. Farmer,
645 and R. C. Cohen (2009), Thermodynamic characterization of Mexico City aerosol during MILAGRO 2006,
646 *Atmos. Chem. Phys.*, *9*(6), 2141-2156, doi:10.5194/acp-9-2141-2009.

647 Ge, X. L., A. Setyan, Y. L. Sun, and Q. Zhang (2012a), Primary and secondary organic aerosols in Fresno,
648 California during wintertime: Results from high resolution aerosol mass spectrometry, *Journal of*
649 *Geophysical Research-Atmospheres*, *117*, 15, doi:10.1029/2012jd018026.

Ge, X. L., Q. Zhang, Y. Sun, C. R. Ruehl, and A. Setyan (2012b), Effect of aqueous-phase processing on aerosol chemistry and size distributions in Fresno, California, during wintertime, *Environmental Chemistry*, *9*(3), 221-235, doi:https://doi.org/10.1071/EN11168.

Gentner, D. R., et al. (2014), Emissions of organic carbon and methane from petroleum and dairy operations in California's San Joaquin Valley, *Atmos. Chem. Phys.*, *14*(10), 4955-4978, doi:10.5194/acp-14-4955-2014.

Herckes, P., A. R. Marcotte, Y. Wang, and J. L. Collett (2015), Fog composition in the Central Valley of California over three decades, *Atmospheric Research*, *151*, 20-30, doi:http://dx.doi.org/10.1016/j.atmosres.2014.01.025.

Herner, J. D., J. Aw, O. Gao, D. P. Chang, and M. J. Kleeman (2005), Size and Composition Distribution of Airborne Particulate Matter in Northern California: I—Particulate Mass, Carbon, and Water-Soluble Ions, *Journal of the Air & Waste Management Association*, *55*(1), 30-51, doi:10.1080/10473289.2005.10464600.

Herner, J. D., Q. Ying, J. Aw, O. Gao, D. P. Y. Chang, and M. J. Kleeman (2006), Dominant Mechanisms that Shape the Airborne Particle Size and Composition Distribution in Central California, *Aerosol Science and Technology*, *40*(10), 827-844, doi:10.1080/02786820600728668.

Hixson, M., A. Mahmud, J. Hu, and M. J. Kleeman (2012), Resolving the interactions between population density and air pollution emissions controls in the San Joaquin Valley, USA, *Journal of the Air & Waste Management Association*, *62*(5), 566-575, doi:10.1080/10962247.2012.663325.

Houyoux, M. R., J. M. Vukovich, C. J. Coats, N. J. M. Wheeler, and P. S. Kasibhatla (2000), Emission inventory development and processing for the Seasonal Model for Regional Air Quality (SMRAQ) project, *Journal of Geophysical Research: Atmospheres*, *105*(D7), 9079-9090, doi:10.1029/1999JD900975.

Jacob, D. J., J. W. Munger, J. M. Waldman, and M. R. Hoffmann (1986), The H2SO4-HNO3-NH3 system at high humidities and in fogs: 1. Spatial and temporal patterns in the San Joaquin Valley of California, *Journal of Geophysical Research: Atmospheres*, *91*(D1), 1073-1088, doi:10.1029/JD091iD01p01073.

Jang, J. C. C., H. E. Jeffries, and S. Tonnesen (1995), Sensitivity of ozone to model grid resolution. 2. Detailed process analysis for ozone chemistry, *Atmospheric Environment*, *29*(21), 3101-3114, doi:10.1016/1352-2310(95)00119-j.

Jeffries, H. E., and S. Tonnesen (1994), A comparison of 2 photochemical-reaction mechanisms using mass-balance and process analysis, *Atmospheric Environment*, *28*(18), 2991-3003, doi:10.1016/1352-2310(94)90345-x.

Kelly, J. T., J. Avise, C. Cai, and A. P. Kaduwela (2011), Simulating Particle Size Distributions over California and Impact on Lung Deposition Fraction, *Aerosol Science and Technology*, *45*(2), 148-162, doi:10.1080/02786826.2010.528078.

Kelly, J. T., K. R. Baker, C. G. Nolte, S. L. Napelenok, W. C. Keene, and A. A. P. Pszenny (2016), Simulating the phase partitioning of NH3, HNO3, and HCl with size-resolved particles over northern Colorado in winter, *Atmospheric Environment*, *131*, 67-77, doi:10.1016/j.atmosenv.2016.01.049.

686 Kelly, J. T., et al. (2014), Fine-scale simulation of ammonium and nitrate over the South Coast Air Basin and
687 San Joaquin Valley of California during CalNex-2010, *Journal of Geophysical Research: Atmospheres*, *119*(6),
688 3600-3614, doi:10.1002/2013JD021290.

689 Kelly, J. T., P. V. Bhave, C. G. Nolte, U. Shankar, and K. M. Foley (2010), Simulating emission and chemical
690 evolution of coarse sea-salt particles in the Community Multiscale Air Quality (CMAQ) model, *Geoscientific*
691 *Model Development*, *3*(1), 257-273.

692 Kelly, J. T., A. S. Wexler, C. K. Chan, and M. N. Chan (2008), Aerosol thermodynamics of potassium salts,
693 double salts, and water content near the eutectic, *Atmospheric Environment*, *42*(16), 3717-3728,
694 doi:10.1016/j.atmosenv.2008.01.001.

695 Kim, Y. J., S. N. Spak, G. R. Carmichael, N. Riemer, and C. O. Stanier (2014), Modeled aerosol nitrate
696 formation pathways during wintertime in the Great Lakes region of North America, *Journal of Geophysical*
697 *Research-Atmospheres*, *119*(21), 12420-12445, doi:10.1002/2014jd022320.

698 Kleeman, M. J., Q. Ying, and A. Kaduwela (2005), Control strategies for the reduction of airborne particulate
699 nitrate in California's San Joaquin Valley, *Atmospheric Environment*, *39*(29), 5325-5341,
700 doi:http://dx.doi.org/10.1016/j.atmosenv.2005.05.044.

701 Livingstone, P. L., et al. (2009), Simulating PM concentration during a winter episode in a subtropical valley:
702 Sensitivity simulations and evaluation methods, *Atmospheric Environment*, *43*(37), 5971-5977,
703 doi:10.1016/j.atmosenv.2009.07.033.

704 Lonsdale, C. R., et al. (2017), Modeling the diurnal variability of agricultural ammonia in Bakersfield,
705 California, during the CalNex campaign, *Atmos. Chem. Phys.*, *17*(4), 2721-2739, doi:10.5194/acp-17-2721-
706 2017.

707 McDonald, B. C., T. R. Dallmann, E. W. Martin, and R. A. Harley (2012), Long-term trends in nitrogen oxide
708 emissions from motor vehicles at national, state, and air basin scales, *Journal of Geophysical Research-*
709 *Atmospheres*, *117*, doi:10.1029/2012jd018304.

710 Meng, Z., and J. H. Seinfeld (1996), Time scales to achieve atmospheric gas-aerosol equilibrium for volatile
711 species, *Atmospheric Environment*, *30*(16), 2889-2900, doi:http://dx.doi.org/10.1016/1352-2310(95)00493-
712 9.

713 Miller, D. J., K. Sun, L. Tao, M. A. Khan, and M. A. Zondlo (2014), Open-path, quantum cascade-laser-based
714 sensor for high-resolution atmospheric ammonia measurements, *Atmospheric Measurement Techniques*,
715 *7*(1), 81-93, doi:10.5194/amt-7-81-2014.

716 Miller, D. J., et al. (2015), Ammonia and methane dairy emission plumes in the San Joaquin Valley of
717 California from individual feedlot to regional scales, *Journal of Geophysical Research: Atmospheres*, *120*(18),
718 9718-9738, doi:10.1002/2015JD023241.

719 Mlawer, E. J., S. J. Taubman, P. D. Brown, M. J. Iacono, and S. A. Clough (1997), Radiative transfer for
720 inhomogeneous atmospheres: RRTM, a validated correlated-k model for the longwave, *Journal of*
721 *Geophysical Research: Atmospheres*, *102*(D14), 16663-16682, doi:10.1029/97JD00237.

722 Morrison, H., G. Thompson, and V. Tatarskii (2009), Impact of Cloud Microphysics on the Development of
723 Trailing Stratiform Precipitation in a Simulated Squall Line: Comparison of One- and Two-Moment Schemes,
724 *Monthly Weather Review*, *137*(3), 991-1007, doi:10.1175/2008mwr2556.1.

725 NASA (2017), Airborne Science Data for Atmospheric Composition, *https://www-air.larc.nasa.gov/cgi-*
726 *bin/ArcView/discover-aq.ca-2013*

727 Nenes, A., S. N. Pandis, and C. Pilinis (1998), ISORROPIA: A New Thermodynamic Equilibrium Model for
728 Multiphase Multicomponent Inorganic Aerosols, *Aquatic Geochemistry*, *4*(1), 123-152,
729 doi:10.1023/a:1009604003981.

730 NOAA (2017), Earth System Research Laboratory Physical Sciences Division.
731 ftp://ftp1.esrl.noaa.gov/psd2/data/realtime/Radar915/CnsWind/vis/2013/ Accessed June 2017.

732 Parworth, C. L., D. E. Young, H. Kim, X. Zhang, C. D. Cappa, S. Collier, and Q. Zhang (2017), Wintertime
733 water-soluble aerosol composition and particle water content in Fresno, California, *Journal of Geophysical*
734 *Research: Atmospheres*, *122*(5), 3155-3170, doi:10.1002/2016JD026173.

735 Pleim, J. E. (2007), A Combined Local and Nonlocal Closure Model for the Atmospheric Boundary Layer. Part
736 I: Model Description and Testing, *Journal of Applied Meteorology and Climatology*, *46*(9), 1383-1395,
737 doi:10.1175/jam2539.1.

738 Pleim, J. E., J. O. Bash, J. T. Walker, and E. J. Cooter (2013), Development and evaluation of an ammonia
739 bidirectional flux parameterization for air quality models, *Journal of Geophysical Research-Atmospheres*,
740 *118*(9), 3794-3806, doi:10.1002/jgrd.50262.

741 Pleim, J. E., and A. Xiu (2003), Development of a Land Surface Model. Part II: Data Assimilation, *Journal of*
742 *Applied Meteorology*, *42*(12), 1811-1822, doi:10.1175/1520-0450(2003)042<1811:doalsm>2.0.co;2.

743 Prabhakar, G., et al. (2017), Observational assessment of the role of nocturnal residual-layer chemistry in
744 determining daytime surface particulate nitrate concentrations, *Atmos. Chem. Phys.*, *17*(23), 14747-14770,
745 doi:10.5194/acp-17-14747-2017.

746 Pun, B. K., R. T. F. Balmori, and C. Seigneur (2009), Modeling wintertime particulate matter formation in
747 central California, *Atmospheric Environment*, *43*(2), 402-409,
748 doi:http://dx.doi.org/10.1016/j.atmosenv.2008.08.040.

749 Pun, B. K., and C. Seigneur (1999), Understanding particulate matter formation in the California San Joaquin
750 Valley: conceptual model and data needs, *Atmospheric Environment*, *33*(29), 4865-4875,
751 doi:http://dx.doi.org/10.1016/S1352-2310(99)00266-6.

752 Pun, B. K., and C. Seigneur (2001), Sensitivity of Particulate Matter Nitrate Formation To Precursor
753 Emissions in the California San Joaquin Valley, *Environmental Science & Technology*, *35*(14), 2979-2987,
754 doi:10.1021/es0018973.

755 Pusede, S. E., and R. C. Cohen (2012), On the observed response of ozone to NOx and VOC reactivity
756 reductions in San Joaquin Valley California 1995-present, *Atmospheric Chemistry and Physics*, *12*(18), 8323-
757 8339, doi:10.5194/acp-12-8323-2012.

Pusede, S. E., et al. (2016), On the effectiveness of nitrogen oxide reductions as a control over ammonium nitrate aerosol, *Atmospheric Chemistry and Physics*, *16*(4), 2575-2596, doi:10.5194/acp-16-2575-2016.

Pusede, S. E., et al. (2014), On the temperature dependence of organic reactivity, nitrogen oxides, ozone production, and the impact of emission controls in San Joaquin Valley, California, *Atmospheric Chemistry and Physics*, *14*(7), 3373-3395, doi:10.5194/acp-14-3373-2014.

Riemer, N., H. Vogel, B. Vogel, B. Schell, I. Ackermann, C. Kessler, and H. Hass (2003), Impact of the heterogeneous hydrolysis of N2O5 on chemistry and nitrate aerosol formation in the lower troposphere under photosmog conditions, *Journal of Geophysical Research: Atmospheres*, *108*(D4), n/a-n/a, doi:10.1029/2002JD002436.

Roberts, J. M., H. D. Osthoff, S. S. Brown, A. R. Ravishankara, D. Coffman, P. Quinn, and T. Bates (2009), Laboratory studies of products of N2O5 uptake on Cl- containing substrates, *Geophysical Research Letters*, *36*, doi:10.1029/2009gl040448.

Russell, A. R., L. C. Valin, and R. C. Cohen (2012), Trends in OMI NO2 observations over the United States: effects of emission control technology and the economic recession, *Atmospheric Chemistry and Physics*, *12*(24), 12197-12209, doi:10.5194/acp-12-12197-2012.

Sarwar, G., H. Simon, P. Bhave, and G. Yarwood (2012), Examining the impact of heterogeneous nitryl chloride production on air quality across the United States, *Atmospheric Chemistry and Physics*, *12*(14), 6455-6473, doi:10.5194/acp-12-6455-2012.

Shephard, M. W., and K. E. Cady-Pereira (2015), Cross-track Infrared Sounder (CrIS) satellite observations of tropospheric ammonia, *Atmospheric Measurement Techniques*, *8*(3), 1323-1336, doi:10.5194/amt-8-1323-2015.

Simon, H., et al. (2010), Modeling heterogeneous ClNO2 formation, chloride availability, and chlorine cycling in Southeast Texas, *Atmospheric Environment*, *44*(40), 5476-5488, doi:10.1016/j.atmosenv.2009.09.006.

SJVAPCD (2012), San Joaquin Valley Air Pollution Control District, 2012 PM2.5 Plan, *Available: http://www.valleyair.org/Air_Quality_Plans/PM25Plans2012.htm*.

SJVAPCD (2016), San Joaquin Valley Air Pollution Control District, 2016 Moderate Area Plan for the 2012 PM2.5 Standard, *Available: http://www.valleyair.org/Air_Quality_Plans/PM25Plans2016.htm*.

Skamarock, W. C., J. B. Klemp, J. Dudhia, D. O. Gill, D. M. Barker, M. G. Duda, X. Huang, W. Wang, and J. G. Powers (2008), A description of the Advanced Reserch WRF version 3. NCAR Technical Note NCAR/TN-475+STR.

Stockwell, W. R., J. G. Watson, N. F. Robinson, W. Steiner, and W. W. Sylte (2000), The ammonium nitrate particle equivalent of NOx emissions for wintertime conditions in Central California's San Joaquin Valley, *Atmospheric Environment*, *34*(27), 4711-4717, doi:https://doi.org/10.1016/S1352-2310(00)00148-5.

Sun, K., et al. (2015), Validation of TES ammonia observations at the single pixel scale in the San Joaquin Valley during DISCOVER-AQ, *Journal of Geophysical Research: Atmospheres*, *120*(10), 5140-5154, doi:10.1002/2014JD022846.

795 Sun, K., L. Tao, D. J. Miller, M. A. Khan, and M. A. Zondlo (2014), On-Road Ammonia Emissions Characterized
796 by Mobile, Open-Path Measurements, *Environmental Science & Technology*, *48*(7), 3943-3950,
797 doi:10.1021/es4047704.

798 USEPA (2012a), CMAQ version 5.0 (February 2012 release) Technical Documentation. Available:
799 https://www.airqualitymodeling.org/index.php/CMAQ_version_5.0_(February_2012_release)_Technical_D
800 ocumentation.

801 USEPA (2012b), Technical Support Document (TSD) Preparation of Emissions Inventories for the Version 5.0,
802 2007 Emissions Modeling Platform. Available: https://www.epa.gov/sites/production/files/2015-
803 10/documents/2007v5_2020base_emismod_tsd_13dec2012.pdf.

804 USEPA (2016), 2011 National Emissions Inventory, version 2. Technical Support Document. Available:
805 https://www.epa.gov/sites/production/files/2015-10/documents/nei2011v2_tsd_14aug2015.pdf.

806 USEPA (2017a), Air Quality System https://www.epa.gov/aqs.

807 USEPA (2017b), Bayesian space-time downscaling fusion model (downscaler)-derived estimates of air
808 quality for 2013.

809 Watson, J. G., and J. C. Chow (2002), A wintertime PM2.5 episode at the Fresno, CA, supersite, *Atmospheric*
810 *Environment*, *36*(3), 465-475, doi:http://dx.doi.org/10.1016/S1352-2310(01)00309-0.

811 Watson, J. G., D. W. DuBois, R. DeMandel, A. Kaduwela, K. L. Magliano, C. McDade, P. K. Mueller, A. J.
812 Ranzieri, P. M. Roth, and S. Tanrikulu (1998), Field program plan for the California Regional PM2.5/PM10Air
813 Quality Study (CRPAQS), *Desert Research Institute, Reno, NV, Available:*
814 *http://www.arb.ca.gov/airways/crpaqs/publications.htm*.

815 Weibring, P., D. Richter, A. Fried, J. G. Walega, and C. Dyroff (2006), Ultra-high-precision mid-IR
816 spectrometer II: system description and spectroscopic performance, *Applied Physics B*, *85*(2), 207-218,
817 doi:10.1007/s00340-006-2300-4.

818 Wexler, A. S., and J. H. Seinfeld (1991), Second-generation inorganic aerosol model, *Atmospheric*
819 *Environment. Part A. General Topics*, *25*(12), 2731-2748, doi:http://dx.doi.org/10.1016/0960-
820 1686(91)90203-J.

821 Womack, C. C., et al. (2017), Evaluation of the accuracy of thermal dissociation CRDS and LIF techniques for
822 atmospheric measurement of reactive nitrogen species, *Atmospheric Measurement Techniques*, *10*(5),
823 1911-1926, doi:10.5194/amt-10-1911-2017.

824 Ying, Q. (2011), Physical and chemical processes of wintertime secondary nitrate aerosol formation,
825 *Frontiers of Environmental Science & Engineering in China*, *5*(3), 348, doi:10.1007/s11783-011-0343-1.

826 Ying, Q., and M. Kleeman (2009), Regional contributions to airborne particulate matter in central California
827 during a severe pollution episode, *Atmospheric Environment*, *43*(6), 1218-1228,
828 doi:http://dx.doi.org/10.1016/j.atmosenv.2008.11.019.

829 Ying, Q., J. Lu, P. Allen, P. Livingstone, A. Kaduwela, and M. Kleeman (2008a), Modeling air quality during
830 the California Regional PM10/PM2.5 Air Quality Study (CRPAQS) using the UCD/CIT source-oriented air

quality model – Part I. Base case model results, *Atmospheric Environment*, *42*(39), 8954-8966, doi:http://dx.doi.org/10.1016/j.atmosenv.2008.05.064.

Ying, Q., J. Lu, A. Kaduwela, and M. Kleeman (2008b), Modeling air quality during the California Regional PM10/PM2.5 Air Quality Study (CPRAQS) using the UCD/CIT Source Oriented Air Quality Model – Part II. Regional source apportionment of primary airborne particulate matter, *Atmospheric Environment*, *42*(39), 8967-8978, doi:http://dx.doi.org/10.1016/j.atmosenv.2008.05.065.

Ying, Q., J. Lu, and M. Kleeman (2009), Modeling air quality during the California Regional PM10/PM2.5 Air Quality Study (CPRAQS) using the UCD/CIT source-oriented air quality model – Part III. Regional source apportionment of secondary and total airborne particulate matter, *Atmospheric Environment*, *43*(2), 419-430, doi:http://dx.doi.org/10.1016/j.atmosenv.2008.08.033.

Young, D. E., H. Kim, C. Parworth, S. Zhou, X. L. Zhang, C. D. Cappa, R. Seco, S. Kim, and Q. Zhang (2016), Influences of emission sources and meteorology on aerosol chemistry in a polluted urban environment: results from DISCOVER-AQ California, *Atmospheric Chemistry and Physics*, *16*(8), 5427-5451, doi:10.5194/acp-16-5427-2016.

Zhang, X. L., H. Kim, C. L. Parworth, D. E. Young, Q. Zhang, A. R. Metcalf, and C. D. Cappa (2016), Optical Properties of Wintertime Aerosols from Residential Wood Burning in Fresno, CA: Results from DISCOVER-AQ 2013, *Environmental Science & Technology*, *50*(4), 1681-1690, doi:10.1021/acs.est.5b04134.

Zhang, Y., P. Liu, X.-H. Liu, B. Pun, C. Seigneur, M. Z. Jacobson, and W.-X. Wang (2010), Fine scale modeling of wintertime aerosol mass, number, and size distributions in central California, *Journal of Geophysical Research: Atmospheres*, *115*(D15), n/a-n/a, doi:10.1029/2009JD012950.

Zhu, L., D. Henze, J. Bash, G. R. Jeong, K. Cady-Pereira, M. Shephard, M. Luo, F. Paulot, and S. Capps (2015), Global evaluation of ammonia bidirectional exchange and livestock diurnal variation schemes, *Atmos. Chem. Phys.*, *15*(22), 12823-12843, doi:10.5194/acp-15-12823-2015.